科技部補助專題研究計畫成果報告
期末報告

探討高體溫引發 Brugada 症候群的細胞及離子流機轉之研究(第 2 年)

計 畫 類 別 ：個別型計畫
計 畫 編 號 ：NSC 101-2314-B-040-017-MY2
執 行 期 間 ：102 年 08 月 01 日至 103 年 07 月 31 日
執 行 單 位 ：中山醫學大學醫學系

計 畫 主 持 人：蔡青峰
共 同 主 持 人：陳亦仁
計畫參與人員：碩士級-專任助理人員：林豐智

處 理 方 式 ：
1.公開資訊：本計畫涉及專利或其他智慧財產權，1 年後可公開查詢
2.「本研究」是否已有嚴重損及公共利益之發現：否
3.「本報告」是否建議提供政府單位施政參考：否

中 華 民 國 103 年 10 月 26 日

中 文 摘 要 ： 造成這種特殊 Brugada 型態的心電圖表現的細胞機轉目前被認為可能是在右心室出口的心外膜心肌細胞在早期再極化過程中淨外向離子流增加所導致。心室出口頻脈是原發性心室頻脈常見位置包含左右心室出口。藉由傳統電極記錄、全細胞膜片箝研究左右心室出口之動作電位及細胞離子流並利用西方墨點記錄離子流及鈣離子調控蛋白質的表現。相較右心室出口左心室出口細胞有較長動作電位期間較大的鈣離子含量及較大的鈉鈣交換離子流但有較小的暫時性外向性鉀離子流(Ito)及延遲性整流型鉀離子通道(Ikr)。右心室出口有較多的鈉鈣離子交換及 ryanodine 接受體蛋白表現但較少的 SERCA2a(內質網 ATPase)蛋白表現。左右心室出口細胞有獨特的電生理特性而具高度心律不整性，且左右心室鉀離子分布差異及不同的鈣離子調控蛋白質的表現。

中文關鍵詞： 布魯格達氏症候群 左右心室出口 心室出口頻脈 細胞離子流 心律不整性

英 文 摘 要 ： Background: The underlying cellular mechanism in Brugada phenotype is proposed to be caused by an outward shift of the ionic currents during early repolarization in right ventricular outflow tract (RVOT) epicardium. Outflow tract ventricular tachyarrhythmia (VT) is the most common form of idiopathic VT typically originating from RVOT but also from the left ventricular outflow tract (LVOT). No information is available on action potential and ionic differences in RVOT versus LVOT comparisons. Methods: Whole-cell patch clamp and indo-1 fluorometric ratio techniques were used to investigate action potentials, Ca2+ homeostasis, and ionic currents in isolated cardiomyocytes from the rabbit RVOT and LVOT. In contrast to RVOTcardiomyocytes, LVOT cardiomyocytes were characterized by longer action potential duration measured at 90% and 50% repolarization, larger Ca2+ transients, higher Ca2+ stores, higher Na+-Ca2+ exchanger currents, and similar L-type Ca2+ currents and late Na+ current, but smaller transient outward K+ currents and delayed rectifier K+ currents. In addition, RVOT had larger expression of sodium-calcium exchanger and ryanodine receptor, but had smaller sarcoplasmic reticulum ATPase than RVA

cardiomyocytes. There were similar expression of Cav1.2, Kir1.5, Kir 2.1 and Kir2.3 between RVOT and RVA. Conclusion: Differences in potassium currents may well explain the interventricular heterogeneity of action potentials in rabbit ventricular outflow tracts. These results contribute to a further phenotyping of the ventricular action potential under physiological conditions. Outflow tracts contain distinctive electrophysiological characteristics with a higher arrhythmogenesis. The regional differences in protein expressions for calcium handling may contribute to the arrhythmogenicity.

英文關鍵詞： Brugada syndrome, left and right outflow tract, ventricular tachycardia, ionic current, arrhythmogenesis

Introduction

A syndrome of sudden death characterized by ST-segment elevation in right precordial leads V1 to V3, unrelated to ischemia or structural heart disease but at times accompanied by a right bundle-branch block morphology of the ECG, was described as a new clinical entity by Pedro and Josep Brugada in 1992 [1]. Brugada syndrome is thought to be an inherited cardiac disorder that predisposes to life-threatening ventricular tachyarrhythmias and sudden cardiac death, especially during sleep or rest, vagal nerve activation and bradycardia [1, 2]. A typical (type I) Brugada ECG pattern is characterized by a distinct coved-type ST-segment elevation (high takeoff > 2 mm) followed by a negative T wave in at least two of the right precordial leads (V1-V3). It is well known that the Brugada ECG pattern is dynamic and might be accentuated or unmasked by certain physiological conditions (e.g. vagal stimulation) or pharmacological challenge (e.g. sodium channel blocker) [2]. The underlying ECG mechanism in Brugada phenotype is hypothesized to be an outward shift of the ionic currents during early repolarization, causing an accentuation of the action potential notch and eventual loss of the action potential dome and marked abbreviation of the action potentials in the **right ventricular outflow** epicardial cells results in ST-segment elevation, phase 2 reentry, and ventricular tachyarrhythmias [3-6]. The proposed mechanism involves a rebalancing of the currents available at the end of phase 1 of the epicardial action potential. Diminution of inward currents (I_{Na} and I_{Ca}) or enhancement of outward currents (I_{to}, $I_{K\text{-}ATP}$, I_{Kr}, I_{Ks}, $I_{Cl(Ca)}$) can result in an accentuation of the epicardial action potential notch as well as all-or-none repolarization at the end of phase 1. Mutations leading to loss of function in I_{Na} and I_{Ca}, as well as those giving rise to a gain of function in I_{to}, have been identified as genetic causes of Brugada syndrome [7-11]. Additionally, any condition or medication that increases outward currents or decreases inward currents may precipitate or unmask Brugada syndrome [12, 13]. Numerous case reports have demonstrating that a febrile state could unmask the Brugada ECG or exacerbate ST-segment elevation and increase arrhythmogenesis [1, 14-20]. However, the prognostic value of Brugada pattern ECG changes observed only during a febrile illness remains unknown. As published reports of the induced Brugada sign have become increasingly prevalent, there is growing interest in the mechanisms responsible for this acquired ECG pattern and its clinical significance [21]. It is possible that the induced Brugada phenotype may be due to an individual susceptibility that favors fever-induced ECG abnormalities, possibly as a result of an increase in a latent ion channel dysfunction similar to that in drug-induced long QT syndrome. It is well recognized that cardiac electrophysiologic properties are temperature sensitive. Electrophysiological studies using in vitro cell expression systems have shown that the increase of temperature going from ambient temperature to high temperature (32℃ to 41℃) can decrease sodium currents by altering ion channel gating kinetics [22-25]. In addition to the effects temperature has on the expression

and function of I_{Na}, temperature is likely to affect other ionic processes responsible for the Brugada ECG phenotype [26]. For example, an increase in heart rate and sympathetic activity during a febrile state would increase inward calcium currents with subsequent prevent the development of Brugada ECG phenotype. Additionally, although changes in I_{to} may not be responsible for precipitating the syndrome in most cases of Brugada syndrome, the presence of a prominent I_{to}-mediated action potential notch appears to be a prerequisite. Indeed, the presence of a much greater I_{to} in right versus left ventricular epicardium accounts for the right ventricular nature of the disease [27]. Moreover, the predominance of the Brugada phenotype in males is a result of the presence of a more prominent I_{to} in males versus females [28]. Therefore, it is plausible that temperature-dependent changes of currents other than I_{Na} could precipitate the Brugada syndrome during fever. Previous studies performed in the canine ventricular wedge preparation have demonstrated that when a further shift in the balance of currents in the early phases of action potentials will result in the development of an epicardial dispersion of repolarization giving rise to a closely coupled phase 2 reentry extrasystole (as trigger), and marked transmural dispersion of repolarization and refractoriness (as substrate) promoting the reentrant arrhythmia [2, 3-6]. However, Lambiase et al. showed that regional conduction delay plays an important role in the initiation and maintenance of ventricular tachyarrhythmias by using non-contact (EnSite) mapping in the Brugada syndrome patients [29]. Recently, it was demonstrated that repolarization or action potential duration alternans, particularly discordant alternans, which is characterized by simultaneous prolongation and shortening of action potential duration in different myocardial regions, is central to the genesis of ventricular arrhythmias [30, 31]. T wave alternant has also been demonstrated in some Brugada syndrome patients [15, 32].Therefore, spatially discordant action potential duration alternans also may be the underlying mechanism of the initiation and maintenance of ventricular arrhythmias in Brugada syndrome. Because fever is a common medical problem, it is critical to study the underlying cellular and ionic mechanisms behind the ECG signature of fever-induced Brugada phenotype to understand how temperature modulates the dynamic and heterogeneity of action potential in the ventricles and what the mechanisms responsible for temperature exacerbation of ventricular arrhythmias in Brugada syndrome are.

Right ventricular outflow tract (RVOT) is an important focus, from which ventricular tachyarrhythmias, such as idiopathic ventricular tachycardia (VT), ventricular arrhythmia with Brugada syndrome, and torsade de pointes, commonly originate [33-35]. Functional dynamics of action potentials (APs) and repolarization heterogeneity in the RVOT are believed to be major contributors to Brugada-type electrocardiographic changes [36, 37]. Outflow tract arrhythmia (VT or frequent VPCs) is the most common form of idiopathic VT and typically originates from the RVOT but can also occur from the left ventricular outflow tract (LVOT), the aortic sinus of Valsalva and the epicardial surface of the ventricles [38–40]. Idiopathic VT can be caused by triggered activity from the RVOT as a consequence of

increased intracellular Ca^{2+} and/or cAMP [41]. Other factors such as electrophysiological heterogeneities existing between the RVOT and right ventricular free wall [42], including regional differences in expression of connexins and ion channels [43], as well as distinct Ca^{2+} handling [44, 45], have been proposed to play an important role in the RVOT arrhythmogenicity. However, the electrophysiological characteristics and Ca^{2+} regulation in RVOT and LVOT cardiomyocytes have not been studied comprehensively.

The purpose of this study in the first year is to investigate the electrophysiological characteristics (action potentials and ionic currents) in the isolated pieces of right ventricular free walls (outflow tract, anterolateral wall near apex), and the effects of drugs and temperature on them before and after drug-induced Brugada model. We intend to delineate the cellular and ionic mechanisms underlying the development of fever-induced Brugada ECG phenotype. In the second year, we investigate the electrophysiological characteristics (action potentials and ionic currents) in the isolated pieces of right and left ventricular outflow tract.

Methods

Electrophysiological study of isolated single cardiomyocytes

This investigation conformed to the institutional Guide for the Care and Use of Laboratory Animals. Single RVOT and LVOT cardiomyocytes were isolated from 25 rabbits (weight 1−2 kg) anesthetized with an intraperitoneal injection of sodium pentobarbital (100 mg/kg). Hearts were removed and mounted on a Langendorff apparatus to be superfused in an antegrade manner with oxygenated normal Tyrode's solution at 37 °C, containing (in mM): NaCl 137, KCl 5.4, $CaCl_2$ 1.8, $MgCl_2$ 0.5, HEPES 10, and glucose 11; adjusted to pH 7.4 with NaOH. After the hearts were cleaned of blood, the perfusate was replaced with an oxygenated Ca^{2+}-free Tyrode's solution containing 300 units/mL of collagenase type I (Sigma, St. Louis, MO, USA) and 0.25 units/mL protease type XIV (Sigma) for 8-12 min. The RVOT (area within 5 mm below the pulmonary valve) and LVOT (area within 5 mm below the aortic valv) were excised, and gently shaken in 50 mL of Ca^{2+}-free oxygenated Tyrode's solution until single cardiomyocytes were obtained. The solution was then gradually changed to normal oxygenated Tyrode's solution. Cardiomyocytes were allowed to stabilize in the bath for at least 30 min before the experiments.

Measurement of intracellular Ca^{2+}

Intracellular Ca^{2+} concentration ($[Ca^{2+}]_i$) was recorded by a fluorometric ratio technique as previously described [46]. The fluorescent indicator, indo-1, was loaded by incubating cardiomyocytes at room temperature for 20−30 min with indo-1/AM (10 μmol/L,

Sigma). Then, cardiomyocytes were then perfused with normal Tyrode's solution at 35 ± 1 ℃ for ≥ 30 min to wash out the extracellular indicator and allow for intracellular deesterification of indo-1. Background and cellular autofluorescence levels were canceled out by zeroing the output of the photomultiplier tubes using cells without indo-1 loading. Ultraviolet light of 360 nm from a monochromator was used to excite indo-1 with a xenon arc lamp controlled by a microfluorometric system (OSP100-CA; Olympus, Tokyo, Japan). The excitation light beam was directed into an inverted microscope (IX-70; Olympus). The emitted fluorescence signals from indo-1/AM-loaded cardiomyocytes were digitized at 200 Hz. We calculated the ratio of fluorescence emissions at 410 and 485 nm. The $R_{410/485}$ value was used as an index of $[Ca^{2+}]_i$ and measured during 1 Hz field stimulation. After achieving a steady-state Ca^{2+} transients with the repeated pulses from -40 to 0 mV (1 Hz for 5 s), the sarcoplasmic reticulum (SR) Ca^{2+} content was estimated by integrating the Na^+-Ca^{2+} exchanger (NCX) current following application of 20 mM of caffeine within 0.5 s during rest with the membrane potential clamped to -40 mV to cause SR Ca^{2+} release. The time integral of NCX current was converted to amoles (10^{-18} moles) of Ca^{2+} released from the SR.

Ionic current measurements

Whole-cell patch clamp was used for single isolated cardiomyocytes with an Axopatch 1D amplifier (Axon Instruments, Foster City, CA, USA) at 35 ± 1 ℃ [46]. The borosilicate glass electrodes (o.d., 1.8 mm) with tip resistances of 3−5 MΩ were used. Before the formation of the membrane-pipette seal, the tip potentials were zeroed in Tyrode's solution. Junction potentials between the bath and pipette solution (9 mV) were corrected for AP recordings. APs were recorded in the current-clamp mode, and ionic currents were measured in the voltage-clamp mode. A small hyperpolarizing step from a holding potential of -50 mV to a testing potential of -55 mV for 80 ms was delivered at the beginning of each experiment. The area under the capacitative currents was divided by the applied voltage step to obtain whole-cell capacitance. Series resistance (R_s) was compensated by 60−80%. APs were elicited from isolated cardiomyocytes without spontaneous activity at a driven rate of 1 Hz for 20 beats. The resting membrane potential (RMP) was measured during the period between the last repolarization and the onset of the subsequent AP. The AP amplitude (APA) was obtained from RMP to the peak of AP depolarization. AP duration at 90%, 50%, and 20% repolarization were respectively measured as the APD_{90}, APD_{50}, and APD_{20}. In cells with 'spike and dome' shape of APs, the magnitude of phase 1 notch was measured as the membrane potential between the peak of phase 0 and the end of phase 1 [28]. Micropipettes were filled with a solution containing (in mM) KCl 20, K aspartate 110, $MgCl_2$ 1, MgATP 5, HEPES 10, EGTA 0.5, LiGTP 0.1, and Na_2 phosphocreatine 5 (pH 7.2 with KOH).

I_{Na} was recorded using 40 ms pulses from a holding potential of -120 mV to the test potentials varying between -80 and 0 mV in 10 mV increments at a frequency of 3 Hz at room temperature (25 ± 1℃) The external solution contained (in mM): NaCl 5, CsCl 133, $MgCl_2$ 2, $CaCl_2$ 1.8, nifedipine 0.002, HEPES 5, and glucose 5 (pH 7.3). Micropipettes were filled with a solution containing (in mM) CsCl 133, NaCl 5, EGTA 10, MgATP 5, TEACl 20, and HEPES 5 (pH 7.3 with CsOH).

$I_{Na\text{-}Late}$ was recorded at room temperature using a step/ramp protocol consisting of a 100 ms step to +20 mV (from a holding potential of -100 mV) followed by a 100 ms ramp from +20 to -100 mV. $I_{Na\text{-}late}$ was measured from the baseline to the peak of the tetrodotoxin (30 μM)-sensitive fraction of the current as described previously [47, 48]. The external solution containing (in mM): NaCl 130, CsCl 5, $MgCl_2$ 1, $CaCl_2$ 1, HEPES 10, and glucose 10 at a pH of 7.4 with NaOH by a step/ramp protocol (-100 mV step to +20 mV for 100 ms, then ramp back to -100 mV over 100 ms). Micropipettes were filled with a solution containing (in mM) CsCl 130, Na_2ATP 4, $MgCl_2$ 1, EGTA 10, and HEPES 5 (pH 7.3 with NaOH).

$I_{Ca\text{-}L}$ was recorded using 300 ms pulses from a holding potential of -50 mV to test potentials varying between -40 and +60 mV in 10 mV increments at a frequency of 0.1 Hz. In the external solution, NaCl and KCl of the normal Tyrode's solution were replaced with TEACl and CsCl, respectively. Micropipettes were filled with a solution containing (in mM) CsCl 130, $MgCl_2$ 1, MgATP 5, HEPES 10, EGTA 10, NaGTP 0.1, and Na_2 phosphocreatine 5 (pH 7.2 with CsOH). Steady-state inactivation of $I_{Ca\text{-}L}$ was evaluated using a standard protocol consisting of a 300 ms pre-pulse and a 150 ms test pulse. Peak current elicited by the test pulse was divided by the maximal current and plotted as a function of pre-pulse voltage. Data points were fitted with a Boltzmann function. Recovery from inactivation of $I_{Ca\text{-}L}$ was assessed using a two-pulse protocol with 200 ms pre- and test pulses (from -80 mV to +10 mV) separated by varying time intervals. Data points were fitted with a single-exponential function.

NCX current was obtained as the nickel-sensitive current by subtracting current in the presence of 10 mM $NiCl_2$ from that in control. The recording protocol consisted of 300 ms pulses ranging from -100 to +100 mV from a holding potential of -40 mV at a frequency of 0.1 Hz. The external solution for the measurement of NCX contained (in mM): NaCl 140, $CaCl_2$ 2, $MgCl_2$1, HEPES 5 and glucose 10 (pH of 7.4). It was supplemented with strophanthidin (10 μM), nitrendipine (10 μM), and niflumic acid (100 μM). Micropipettes were filled with a solution containing (in mM) NaCl 20, CsCl 110, $MgCl_2$ 0.4, $CaCl_2$ 1.75, tetraethylammonium 20, 1,2-bis(2-aminophenoxy)ethane-N,N,N',N'-tetraacetic acid (BAPTA) 5, glucose 5, MgATP 5 and HEPES 10 (pH of 7.25).

I_{to} was studied using a protocol consisting of a 30 ms pre-pulse from a holding potential of -80 to -40 mV to inactivate sodium channels followed by a 300 ms test pulse to +60 mV in 10 mV increments at a frequency of 0.1 Hz in the presence of 200 μM $CdCl_2$ in Ca^{2+}-free normal Tyrode's solution as described previously [49]. Micropipettes were filled with the same as that used to record APs. I_{to} was measured as the difference between the peak outward current and the steady-state current. Steady-state inactivation of I_{to} was evaluated using a standard protocol consisting of a 1 s pre-pulse and a 0.15 s test pulse. Peak current elicited by the test pulse was divided by the maximal current and plotted as a function of pre-pulse voltage. Data points were fitted with a Boltzmann function. Recovery from inactivation of I_{to} was assessed using a two-pulse protocol with 200 ms pre- and test pulses (from -80 mV to +50 mV) separated by varying time intervals. Data points were fitted with a single-exponential function.

$I_{Kr\text{-}tail}$ was measured as the outward peak tail current density following a 3 s pre-pulse from a holding potential of -40 mV to voltage between -40 and +60 mV in 10 mV steps at a frequency of 0.1 Hz in the presence of chromanol 293B (30 μM) and $CdCl_2$ (200 μM) in the Ca^{2+}-free normal Tyrode's solution. Micropipettes were filled with a solution containing (in mM) KCl 120, $MgCl_2$ 5, $CaCl_2$ 0.36, EGTA 5, HEPES 5, glucose 5, K_2-ATP 5, Na_2-CrP 5, Na-GTP 0.25 (pH 7.2 with KOH).

Western blot of calcium regulation and ionic proteins in RVOT and LVOT

Equal amounts of proteins were resolved by sodium dodecylsulfate polyacrylamide gel electrophoresis as described previously. Blots were probed with antibodies against Cav1.2 ((ICa-L subunit; Alomone Labs, Jerusalem, Israel), SERCA2a (Santa Cruz Biotechnology, CA, USA), Na^+-Ca^{2+} exchanger (NCX; Swant, Bellizona, Switzerland), ryanodine receptor type 2 (RyR2; Affinity Bioreagents, Golden, CO, USA), phospholamban (PLB; Thermo, Rockford, IL, USA), inward rectifier K channel (Kir)1.5 (Alomone Labs), Kir 2.1 (Millipore, Temecula, CA, USA), and Kir2.3 (Millipore) and secondary antibodies conjugated with horseradish peroxidase (Leinco Technology, St. Louis, MO, USA). Bound antibodies were detected with an enhanced chemiluminescence detection system (Millipore, St. Louis, MO, USA) and analyzed with AlphaEaseFC software (Alpha Innotech, San Leandro, CA, USA). Targeted bands were normalized to cardiac α-sarcomeric actin (Sigma-Aldrich, St. Louis, MO, USA) to confirm equal protein loading.

Statistical analysis

All quantitative results are shown as the mean ± standard error of the mean (S.E.M.). Statistical significance between different groups was determined using a paired or unpaired *t*-test, depending on the results of the normality test. Nominal variables were compared by a

Chi-squared analysis with Pearson's correlation. A value of $P < 0.05$ was considered statistically significant.

Results

Electrophysiological characteristics and Ca^{2+} homeostasis of RVOT and LVOT cardiomyocytes

As shown in Fig. 1, LVOT cardiomyocytes had longer APD_{90} (467±27 ms vs. 327±46 ms, $P<0.05$) and APD_{50} (372±23 ms vs. 251±31 ms, $P<0.05$) than RVOT cardiomyocytes. LVOT and RVOT cardiomyocytes had similar values for APD_{20} (194±14 ms vs. 143±19 ms, $P=0.055$), APA (130±1 mV vs. 127±2 mV, $P>0.05$), and RMP (76±1 mV vs. 75±1 mV, $P>0.05$).

We also found that $[Ca^{2+}]_i$ transients are on average by 26% larger in LVOT cardiomyocytes (0.25±0.01 vs. 0.19±0.01 , $P<0.05$) than in RVOT cardiomyocytes, and that LVOT cardiomyocytes are characterized by a relatively fast decay of $[Ca^{2+}]_i$ transients (130±27 ms vs. 256±49 ms , $P<0.05$). The SR Ca^{2+} content was larger in LVOT cardiomyocytes than in RVOT cardiomyocytes. These differences suggest that LVOT and RVOT cardiomyocytes have different electrical activity and Ca^{2+} homeostasis.

Next, we examined ionic currents accounting for the differences between LVOT and RVOT in AP morphology and Ca^{2+} homeostasis. LVOT and RVOT cardiomyocytes had similar current densities of I_{Na} , which could explain the similar APA in LVOT and RVOT cardiomyocytes. To identify the ionic currents responsible for the longer APD in LVOT cardiomyocytes, $I_{Na\text{-}Late}$ and $I_{Ca\text{-}L}$ (inward currents) and potassium channels (outward currents) have been compared. LVOT and RVOT cardiomyocytes had similar current densities of $I_{Na\text{-}Late}$ (Fig. 2) and $I_{Ca\text{-}L}$ (Fig. 3). LVOT cardiomyocytes had a larger NCX (reverse mode) current than RVOT cardiomyocytes (Fig. 4).

Compared to LVOT cardiomyocytes, RVOT cardiomyocytes had a larger I_{to} (Fig. 5) and a larger $I_{Kr\text{-}tail}$ (Fig. 6) . It is feasible that the differences in the properties of ionic currents might contribute to the differences in APD and Ca^{2+} homeostasis between RVOT and LVOT cardiomyocytes.

Western blot analysis in RVOT and RVA

As shown in Figure 7, RVOT had larger expressions of NCX protein and RyR protein than RVA ($P<0.05$), and had a smaller expression of SERCA2a protein than in RVA ($P<0.05$). However, the protein expressions of $Ca_v1.2$, PLB, Kir1.5, Kir2.1, and Kir 2.3 were similar between RVOT and RVA.

Discussion

Idiopathic VT, which is characterized as repetitive monomorphic VT, is not an uncommon form of ventricular arrhythmia in normal structural heart. Outflow tract arrhythmia is the most common form of idiopathic VT and typically originates from the RVOT but can also occur from the left ventricular outflow tract (LVOT. Lerman *et al*. demonstrated that sustained monomorphic VT reproducibly initiated by programmed stimulation to increase $[Ca^{2+}]_i$. Moreover, incremental electrical stimuli induced triggered beats in RVOT suggests that the intracellular calcium has an important role in generating ventricular arrhythmias and implies the different calcium handling characteristics in RVOT. Calcium handling proteins serve an important role in the development of cardiac arrhythmias. In the present study, RVOT had relative high NCX expression, lower expressions of SERCS2a, and enhanced RyR protein expressions than RVA, which augmented the accumulation of $[Ca^{2+}]_i$ as well as diastolic Ca^{2+} in RVOT. It may results in the higher arrhythmogenesis of ouabain in RVOT. Moreover, this study found that the expression of $Ca_v1.2$ and Kir1.5, Kir2.1, and Kir2.3 were similar between RVOT and RVA. The similar Kir2.1 may contribute to the similar RMP between RVA and RVOT. Moreover, we also found that $[Ca^{2+}]_i$ transients and SR Ca^{2+} content are larger in LVOT cardiomyocytes than in RVOT cardiomyocytes. LVOT had relative higher NCX (reverse mode) current but a similar $I_{Ca\text{-}L}$ current density suggestive of higher diastolic Ca^{2+} in LVOT.

For interventricular comparisons of action potentials and corresponding ionic currents, we isolated myocytes from the subepicardial layers of the RV and LV outflow tract of the same rabbit hearts. Our results show that action potentials have a deeper notch, a shorter duration, and less prolongation on slowing of the pacing rate in RVOT than in LVOT cells. A longer APD in the LV versus RV has already been recorded in dogs, both in vitro and in vivo (in dogs with complete atrioventricular block). Taken together, these data indicate that a larger LVOT than RVOT APD exists at normal heart rates and during bradycardia.

Densities of $I_{Na\text{-}Late}$ and $I_{Ca\text{-}L}$ were similar in both ventricular outflow tracts. *I*Kr and I_{to} densities, however, were significantly larger in RVOT, and this difference could explain, at least in part, why APD50 and APD95 were longer and why the APD/pacing CL relationship was steeper in LVOT than in RVOT cells. Heterogeneity of *I*K across the transmural LV wall has been linked to dispersion of repolarization and the danger of torsade de pointes. Our results on *I*Kr (and *Ito*) suggest that arrhythmogenic electromotive gradients could also arise at the junction of the RVOT and LVOT.

Our finding of a large *Ito* in RVOT cells is in keeping with the prominent spike-and-dome morphology of the action potentials. Yan and Antzelevitch presented evidence that the distribution of *Ito* across the canine ventricular wall is causally linked to the J wave of the ECG. Furthermore, this may have important consequences for our

understanding of the Brugada syndrome. ST-segment elevation in the right precordial ECG leads of patients suffering from this disorder has been linked to the concept of "all-or-none repolarization" in the RVOT epicardium.

References

1. Brugada P, Brugada J. Right bundle branch block, persistent ST segment elevation and sudden cardiac death: a distinct clinical and electrocardiographic syndrome: a multicenter report. *J Am Coll Cardiol*. 1992;20:1391–1396.
2. Antzelevitch C, Brugada P, Borggrefe M, Brugada J, Brugada R, Corrado D, Gussak I, LeMarec H, Nademanee K, Perez Riera AR, Shimizu W, Schulze-Bahr E, Tan H, Wilde A: Brugada syndrome: Report of the second consensus conference. Endorsed by the Heart Rhythm Society and the European Heart Rhythm Association. Circulation 2005;111:659-670.
3. Yan GX, Antzelevitch C. Cellular basis for the Brugada syndrome and other mechanisms of arrhythmogenesis associated with ST segment elevation. *Circulation*. 1999;100:1660–1666.
4. Antzelevitch C. The Brugada syndrome: ionic basis and arrhythmia mechanisms. *J Cardiovasc Electrophysiol*. 2001;12:268–272.
5. Fish JM, Antzelevitch C. Role of sodium and calcium channel block in unmasking the Brugada syndrome. Heart Rhythm 2004;1:210–7.
6. Calloe K, Cordeiro JM, Di Diego JM, Hansen RS, Grunnet M, Olesen SP, et al. A transient outward potassium current activator recapitulates the electrocardiographic manifestations of Brugada syndrome. Cardiovasc Res Mar 1 2009;81(4):686–94.
7. Rook MB, Bezzina Alshinawi C, Groenewegen WA, van Gelder I, van Ginneken AC, Jongsma HJ, et al. Human SCN5A gene mutations alter cardiac sodium channel kinetics and are associated with the Brugada syndrome. Cardiovasc Res 1999;44:507–17.
8. Weiss R, Barmada MM, Nguyen T, et al. Clinical and molecular heterogeneity in the Brugada syndrome: a novel gene locus on chromosome 3. *Circulation*. 2002;105:707–713.
9. London B, Michalec M, Mehdi H, Zhu X, Kerchner L, Sanyal S, Viswanathan PC, Pfahnl AE, Shang LL, Madhusudanan M, Baty CJ, Lagana S, Aleong R, Gutmann R, Ackerman MJ, McNamara DM, Weiss R, Dudley SC Jr: Mutation in glycerol-3-phosphate dehydrogenase 1 like gene (GPD1-L) decreases cardiac Na^+ current and causes inherited arrhythmias. Circulation 2007;116:2260-2268.
10. Burashnikov E, Pfeiffer R, Barajas-Martinez H, Delpon E, Hu D, Desai M, BorggrefeM,Haissaguerre M, Kanter R, Pollevick GD, Guerchicoff A, Laino R,Marieb M, Nademanee K, Nam GB, Robles R, Schimpf R, Stapleton DH, Viskin S, Winters S,

Wolpert C, Zimmern S, Veltmann C, Antzelevitch C: Mutations in the cardiac L-type calcium channel associated J wave sydnrome and sudden cardiac death. Heart Rhythm 2010;7:1872-1882.

11. Giudicessi JR, Ye D, Tester DJ, Crotti L, Mugione A, Nesterenko VV, Albertson RM, Antzelevitch C, Schwartz PJ, AckermanMJ: Transient outward current (Ito) gain-of-function mutations in the KCND3-encoded Kv4.3 potassium channel and Brugada syndrome. Heart Rhythm 2011;8:1024-1032.
12. Shimizu W: Acquired forms of Brugada syndrome. In: Antzelevitch C, ed. The Brugada Syndrome: From Bench to Bedside. Oxford, UK: Blackwell Futura, 2004, pp. 166-177.
13. Goldgran-Toledano D, Sideris G, Kevorkian JP: Overdose of cyclic antidepressants and the Brugada syndrome. N Engl J Med 2002;346:1591-1592.
14. Saura D, García-Alberola A, Carrillo P, Pascual D, Martínez-Sánchez J, Valdés M. Brugada-like electrocardiographic pattern induced by fever. Pacing Clin Electrophysiol 2002;25:856–859.
15. Ortega-Carnicer J, Benezet J, Ceres F. Fever-induced ST-segment elevation and T-wave alternans in a patient with Brugada syndrome. Resuscitation 2003;57:315–317.
16. Patruno N, Pontillo D, Achilli A, Ruggeri G, Critelli G. Electrocardiographic pattern of Brugada syndrome disclosed by a febrile illness: clinical and therapeutic implications. Europace 2003;5:251–255.
17. Aramaki K, Okumura M, Shimizu M. Chest pain and ST elevation associated with fever in patients with asymptomatic Brugada syndrome: fever and chest pain in Brugada syndrome. Int J Cardiol 2005;103:338 –339.
18. Amin AS, Meregalli PG, Bardai A, Wilde AA, Tan HL. Fever increases the risk for cardiac arrest in the Brugada syndrome. Ann Intern Med 2008;149:216-8.
19. Junttila MJ, Gonzalez M, Lizotte E, et al. Induced Brugada-type electrocardiogram, a sign for imminent malignant arrhythmias. Circulation 2008;117:1890–1893.
20. Kalra S, Iskandar SB, Duggal S, Smalligan RD. Fever-induced ST-segment elevation with a Brugada syndrome type electrocardiogram. Ann Intern Med 2008;148:82– 84.
21. Yap YG, Behr ER, Camm AJ. Drug-induced Brugada syndrome. Europace 2009;11:989-994.
22. Dumaine R, Towbin JA, Brugada P, et al. Ionic mechanisms responsible for the electrocardiographic phenotype of the Brugada syndrome are temperature dependent. *Circ Res*. 1999;85:803–809.
23. Mok NS, Priori SG, Napolitano C, Chan NY, Chahine M, Baroudi G. A newly characterized SCN5A mutation underlying Brugada syndrome unmasked by hyperthermia. J Cardiovasc Electrophysiol 2003;14:407– 11.
24. Keller DI, Rougier JS, Kucera JP, et al. Brugada syndrome and fever: genetic and molecular characterization of patients carrying SCN5A mutations. Cardiovasc Res

2005;67:510 –519.
25. Samani K, Wu G, Ai T, et al. A novel SCN5A mutation V134OI in Brugada syndrome augmenting arrhythmias during febrile illness. Heart Rhythm 2009;6:1318-1326.
26. Morita H, Zipes DP, Morita ST, Wu J. Temperature modulation of ventricular arrhythmogenicity in canine tissue model of Brugada syndrome. Heart Rhythm 2007;4:188-197.
27. Di Diego JM, Sun ZQ, Antzelevitch C. Ito and action potential notch are smaller in left vs. right canine ventricular epicardium. Am J Physiol. 1996;271:H548–H561.
28. Di Diego JM, Cordeiro JM, Goodrow RJ, Fish JM, Zygmunt AC, Per´ez GJ, Scornik FS, Antzelevitch C: Ionic and cellular basis for the predominance of the Brugada syndrome phenotype in males. Circulation 2002;106:2004-2011.
29. Lambiase PD, Ahmed AK, Ciaccio EJ, Brugada R, Lizotte E, Chaubey S, etal. High-density substrate mapping in Brugada syndrome. Combined role of conduction and repolarization heterogeneities in arrhythmogenesis. Circulation 2009;120:106-117.
30. Pastore JM, Girouard SD, Laurita KR, Akar FG, Rosenbaum DS. Mechanism linking T-wave alternans to the genesis of cardiac fibrillation. Circulation 1999;99:1385–1394.
31. Sato D, Shiferaw Y, Garfinkel A, Weiss JN, Qu Z, Karma A. Spatially discordant alternans in cardiac tissue: role of calcium cycling. Circ Res 2006;99:520 –527.
32. Tada T, Kusano KF, Nagase S, Banba K, Miura D, Nishii N, et al. Clinical significance of macroscopic T-wave alternans after sodium channel blocker administration in patients with Brugada syndrome. J Cardiovasc Electrophysiol 2008;19:56–61.
33. Tsai CF, Chen SA, Tai CT, *et al.* Idiopathic monomorphic ventricular tachycardia: clinical outcome, electrophysiologic characteristics and long-term results of catheter ablation. *Int J Cardiol.* 1997; **62**: 143-50.
34. Kim RJ, Iwai S, Markowitz SM, *et al.* Clinical and electrophysiological spectrum of idiopathic ventricular outflow tract arrhythmias. *J Am Coll Cardiol.* 2007; **49**: 2035-43.
35. Morita H, Fukushima-Kusano K, Nagase S, *et al*. Site-specific arrhythmogenesis in patients with Brugada syndrome. *J Cardiovasc Electrophysiol.* 2003; **14**: 373-9.
36. Morita H, Zipes DP, Morita ST, et al. Differences in arrhythmogenicity between the canine right ventricular outflow tract and anteroinferior right ventricle in a model of Brugada syndrome. *Heart Rhythm* 2007; **4**: 66-74.
37. Morita H, Zipes DP, Fukushima-Kusano K, *et al*. Repolarization heterogeneity in the right ventricular outflow tract: correlation with ventricular arrhythmias in Brugada patients and in an in vitro canine Brugada model. *Heart Rhythm* 2008; **5**: 725-33.
38. Ouyang F, Fotuhi P, Ho SY, et al. Repetitive monomorphic ventricular tachycardia originating from the aortic sinus cusp: electrocardiographic characterization for guiding catheter ablation. J Am Coll Cardiol 2002;39:500–8.
39. Kanagaratnam L, Tomassoni G, Schweikert R, et al. Ventricular tachycardias arising

from the aortic sinus of valsalva: an under-recognized variant of left outflow tract ventricular tachycardia. J Am Coll Cardiol 2001;37:1408–14.

40. Kamakura S, Shimizu W, Matsuo K, et al. Localization of optimal ablation site of idiopathic ventricular tachycardia from right and left ventricular outflow tract by body surface ECG. Circulation 1998;98:1525–33.
41. Lerman BB, Stein K, Engelstein ED, *et al*. Mechanism of repetitive monomorphic ventricular tachycardia. *Circulation* 1995; **92**: 421-9.
42. Watanabe T, Delbridge LM, Bustamante JO, *et al.* Heterogeneity of the action potential in isolated rat ventricular myocytes and tissue. *Circ Res.* 1983; **52**: 280-90.
43. Szentadrassy N, Banyasz T, Biro T, *et al.* Apico-basal inhomogeneity in distribution of ion channels in canine and human ventricular myocardium. *Cardiovasc Res*. 2005; **65**: 851-60.
44. Maury P. Why is the right ventricular outflow tract so arrhythmogenic? (... or is it really?...). *Heart* 2011; **97**: 1631-3.
45. Liang S, Lin C, Li Y, *et al.* L-type calcium current in right ventricular outflow tract myocytes of rabbit heart. *Sci China Life Sci*. 2012; **55**: 41-6.
46. Tsai CF, Chen YC, Lin YK, Chen SA, Chen YJ. Electromechanical effects of the direct renin inhibitor (aliskiren) on the pulmonary vein and atrium. Basic Res Cardiol 2011;106(6):979-993.
47. Lu YY, Chen YC, Kao YH, *et al.* Extracellular matrix of collagen modulates arrhythmogenic activity of pulmonary veins through p38 MAPK activation. *J Mol Cell Cardiol.* 2013; **59**: 159-66.
48. Lin YK, Chen YC, Chen JH, *et al.* Adipocytes modulate the electrophysiology of atrial myocytes: implications in obesity-induced atrial fibrillation. *Basic Res Cardiol*. 2012; 107: 293.

Figure Legends

Figure 1. Action potential (AP) characteristics of the right ventricular outflow tract (RVOT) and left ventricular out-flow tract (LVOT) cardiomyocytes.

Figure 2. Late sodium current (INa-Late) in right ventricular outflow tract (RVOT) and left ventricular out-flow tract (LVOT) cardiomyocytes. The examples of current tracing and average data of INa-Late in RVOT and LVOT cardiomyocytes. Insets in the current traces show the clamp protocol.

Figure 3. Nickel-sensitive Na+-Ca2+ exchanger (NCX) in right ventricular outflow tract (RVOT) and left ventricular out-flow tract (LVOT) cardiomyocytes. Panels show the example of current traces and I–V relationship the ICa-L in RVOT and LVOT.

Figure 4. L-type Ca2+ current (ICa-L) in right ventricular outflow tract (RVOT) and left ventricular out-flow tract (LVOT) cardiomyocytes. The example of current traces and I–V relationship of NCX in RVOT and LVOT cardiomyocytes. Insets show the clamp protocol.

Figure 5. Ito current in right ventricular outflow tract (RVOT) and left ventricular out-flow tract (LVOT) cardiomyocytes. The example of current traces and I–V relationship of Ito in RVOT and LVOT cardiomyocytes. Insets show the clamp protocol.

Figure 6. Ikr-tail current in right ventricular outflow tract (RVOT) and left ventricular out-flow tract (LVOT) cardiomyocytes. The example of current traces and I–V relationship of Ikr-tail in RVOT and LVOT cardiomyocytes. Insets show the clamp protocol.

Figure 7. Western blot analysis of the different calcium-handling protein expressions in RVOT and RVA. RVOT had larger expressions of NCX protein and RyR protein than RVA ($P<0.05$), and had a smaller expression of SERCA2a protein than in RVA ($P<0.05$). However, the protein expressions of $Ca_v1.2$, PLB, Kir1.5, Kir2.1, and Kir 2.3 were similar between RVOT and RVA.

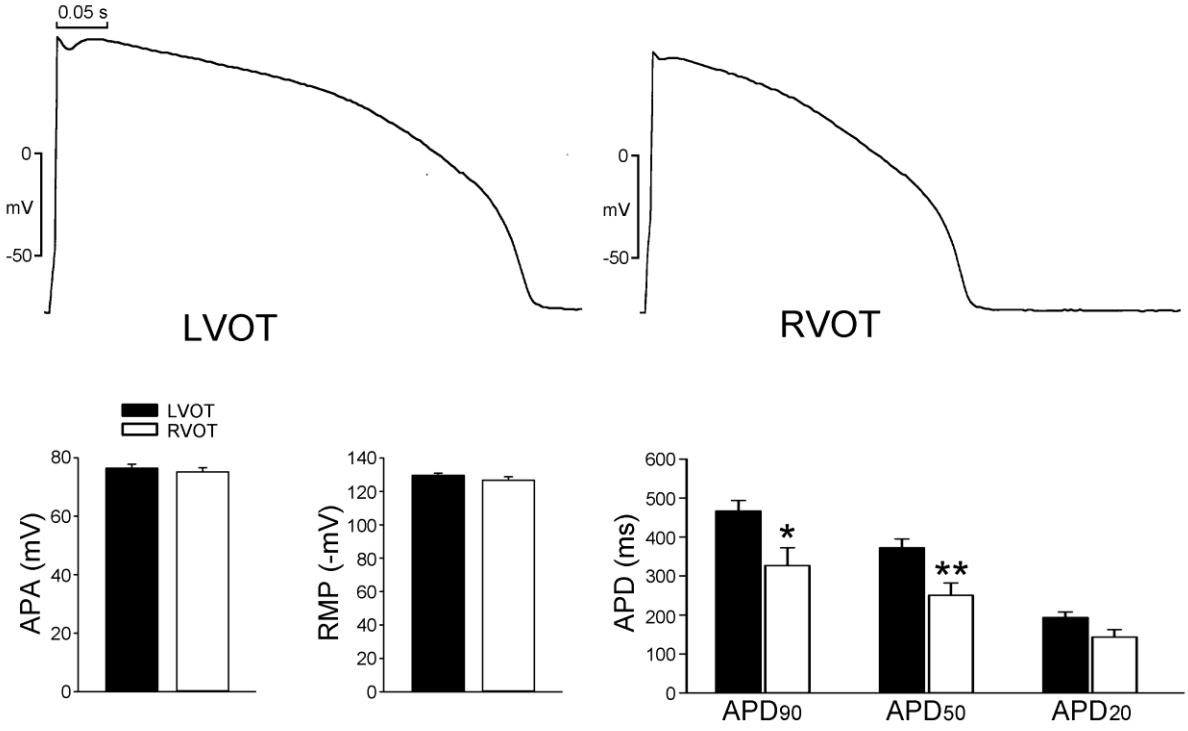
0.05 s
0
mV
-50
LVOT
0
mV
-50
RVOT
LVOT
RVOT
APA (mV)
80
60
40
20
0
RMP (-mV)
140
120
100
80
60
40
20
0
APD (ms)
600
500
400
300
200
100
0
*
**
APD90
APD50
APD20

Figure 1

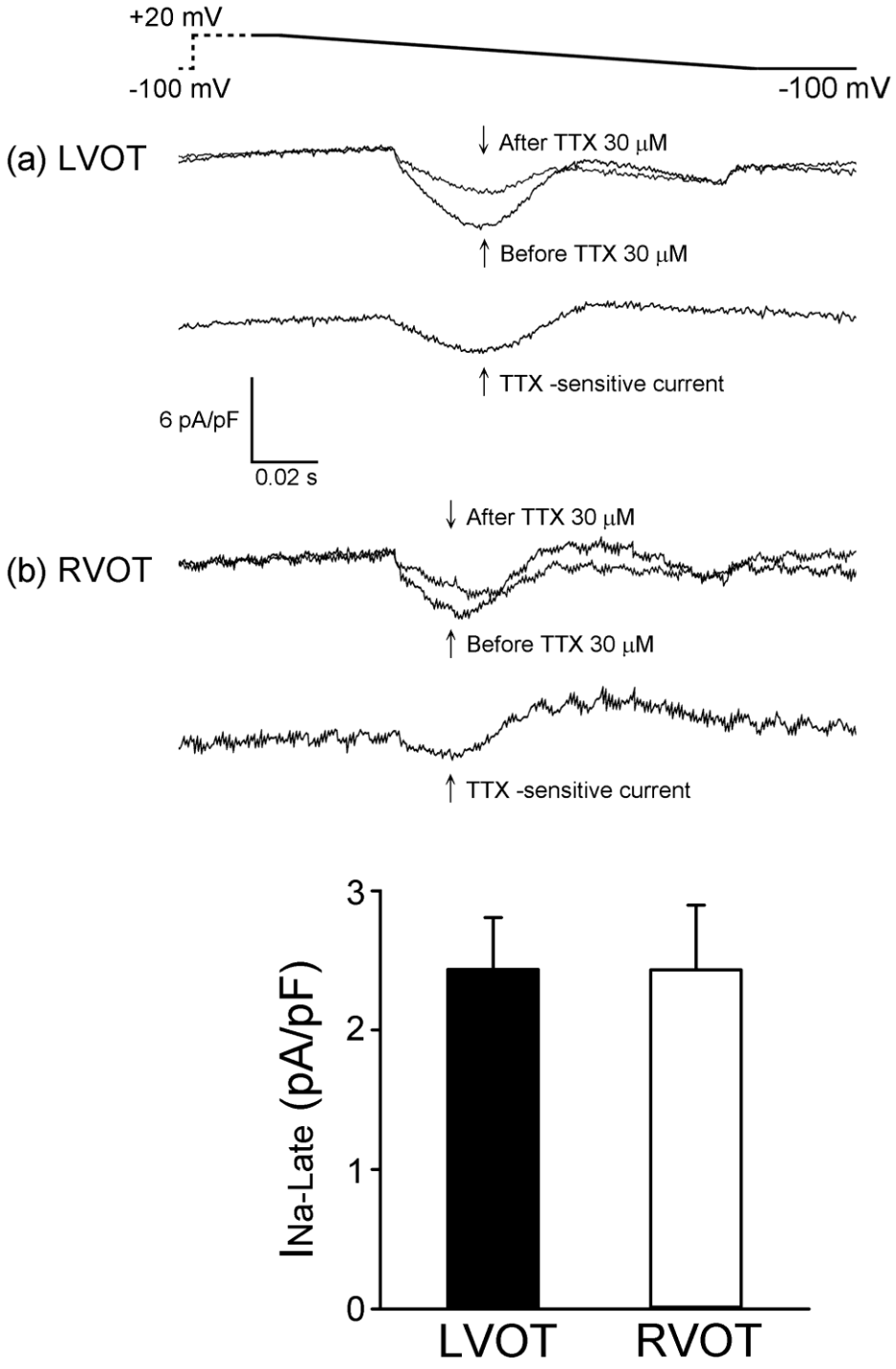
+20 mV
-100 mV
-100 mV
(a) LVOT
After TTX 30 μM
Before TTX 30 μM
TTX -sensitive current
6 pA/pF
0.02 s
(b) RVOT
After TTX 30 μM
Before TTX 30 μM
TTX -sensitive current
INa-Late (pA/pF)
3
2
1
0
LVOT
RVOT

Figure 2

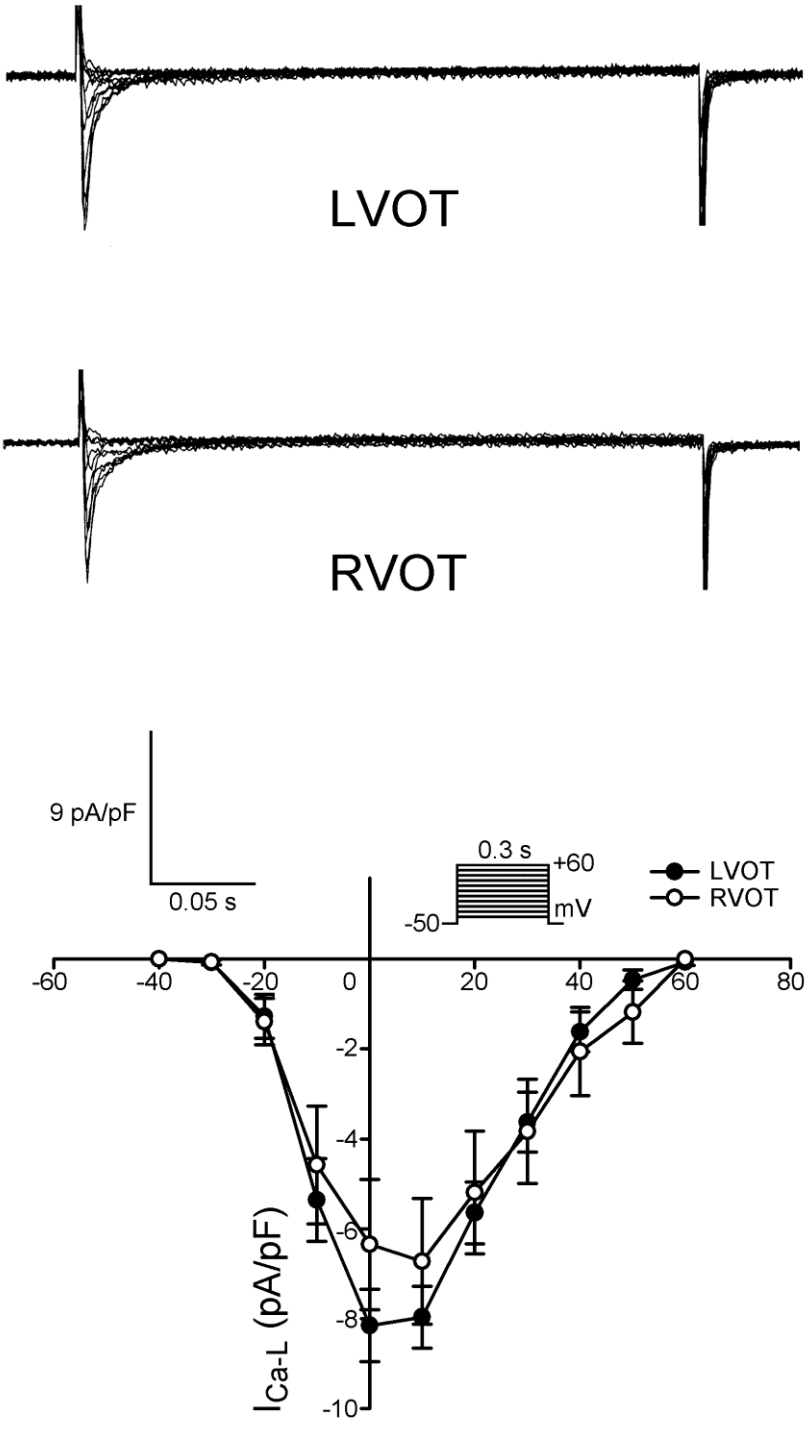
LVOT
RVOT
9 pA/pF
0.05 s
0.3 s
+60
mV
-50
LVOT
RVOT
-60
-40
-20
0
20
40
60
80 (mV)
-2
-4
-6
-8
-10
$I_{Ca\text{-}L}$ (pA/pF)

Figure 3

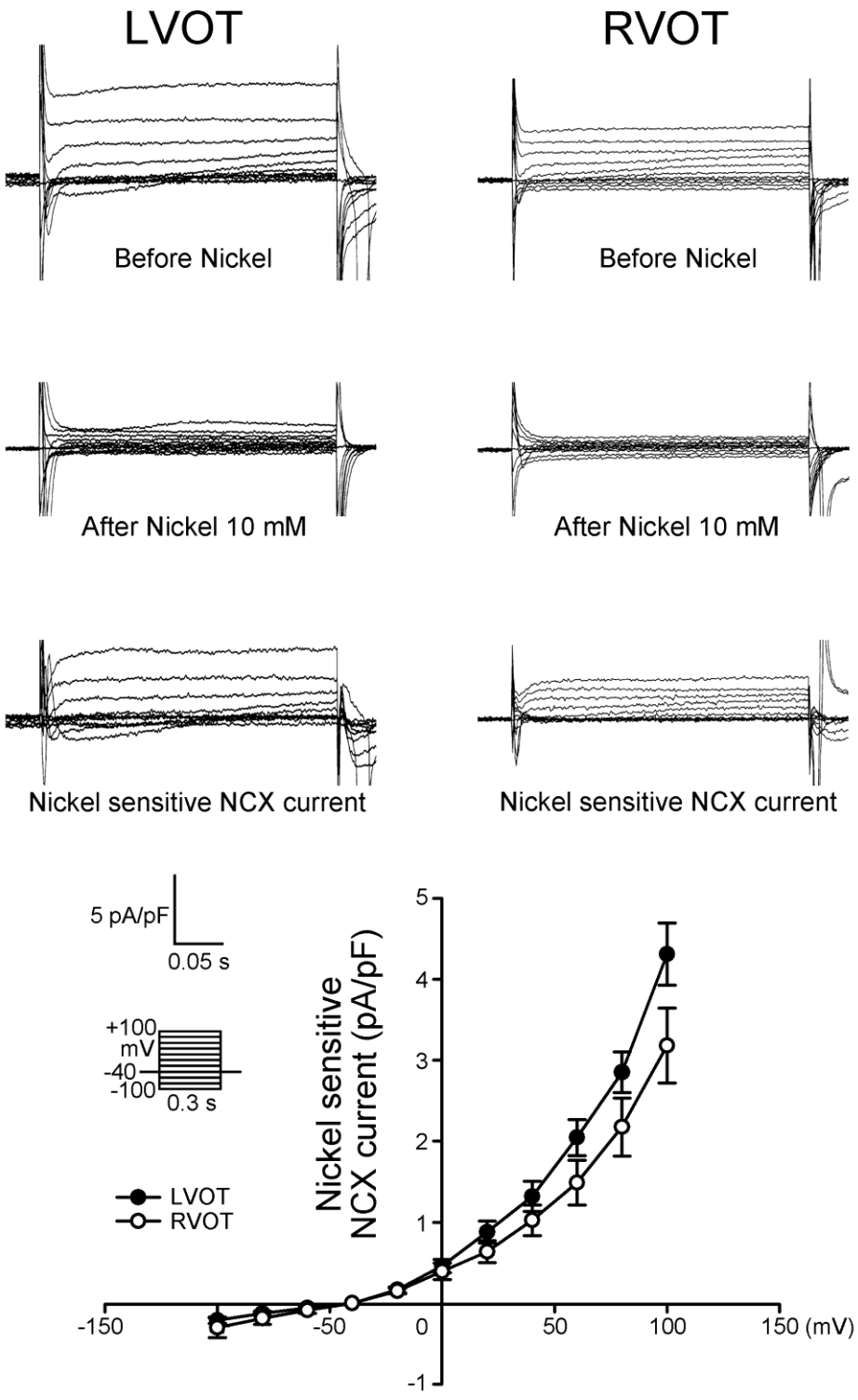
LVOT
RVOT
Before Nickel
Before Nickel
After Nickel 10 mM
After Nickel 10 mM
Nickel sensitive NCX current
Nickel sensitive NCX current
5 pA/pF
0.05 s
+100
mV
-40
-100
0.3 s
LVOT
RVOT
Nickel sensitive
NCX current (pA/pF)
5
4
3
2
1
-1
-150
-50
0
50
100
150 (mV)

Figure 4

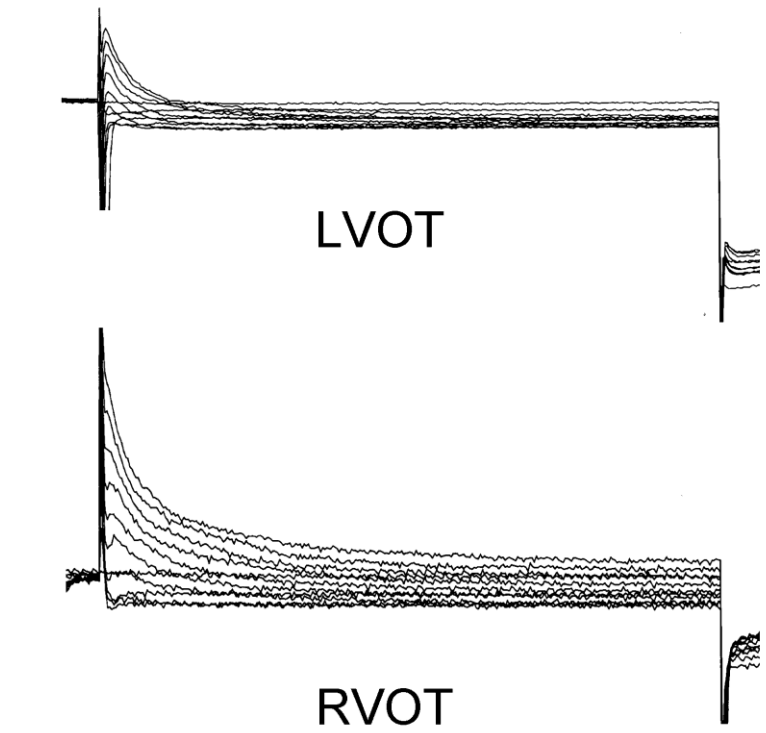
LVOT
RVOT

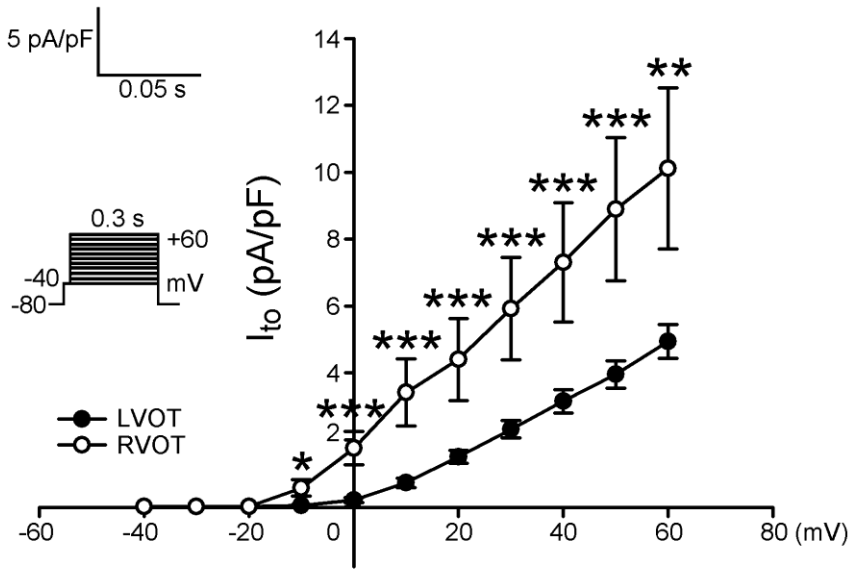
5 pA/pF
0.05 s
0.3 s
+60
-40
mV
-80
LVOT
RVOT
I_{to} (pA/pF)
14
12
10
8
6
4
2
*
***
***
***
***
***
**
-60
-40
-20
0
20
40
60
80 (mV)

Figure 5

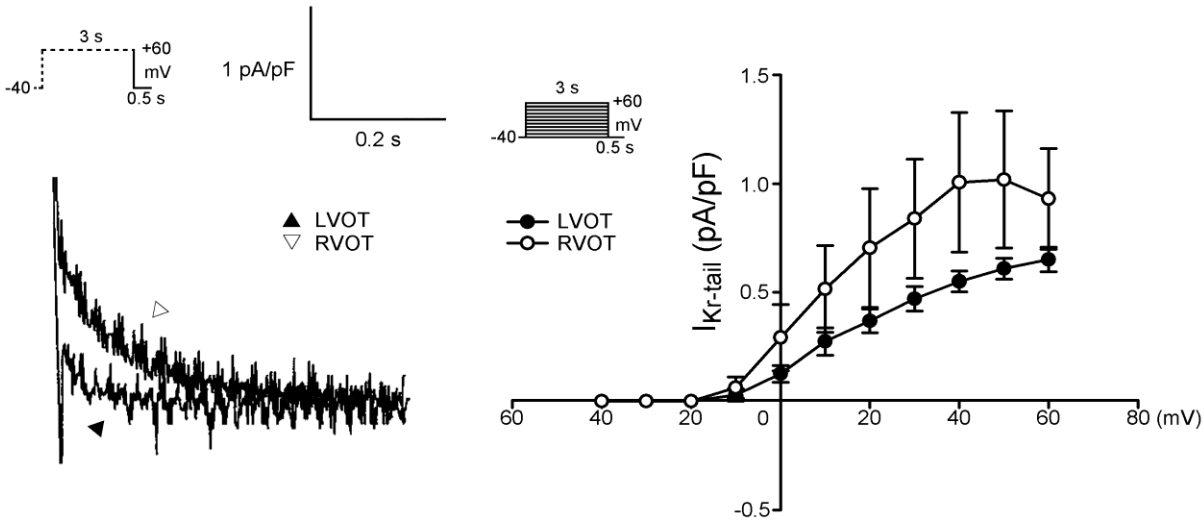
3 s
+60
mV
-40
0.5 s
1 pA/pF
0.2 s
LVOT
RVOT
3 s
+60
mV
-40
0.5 s
LVOT
RVOT
$I_{Kr\text{-}tail}$ (pA/pF)
1.5
1.0
0.5
-0.5
60
40
20
0
20
40
60
80 (mV)

Figure 6

Figure 7

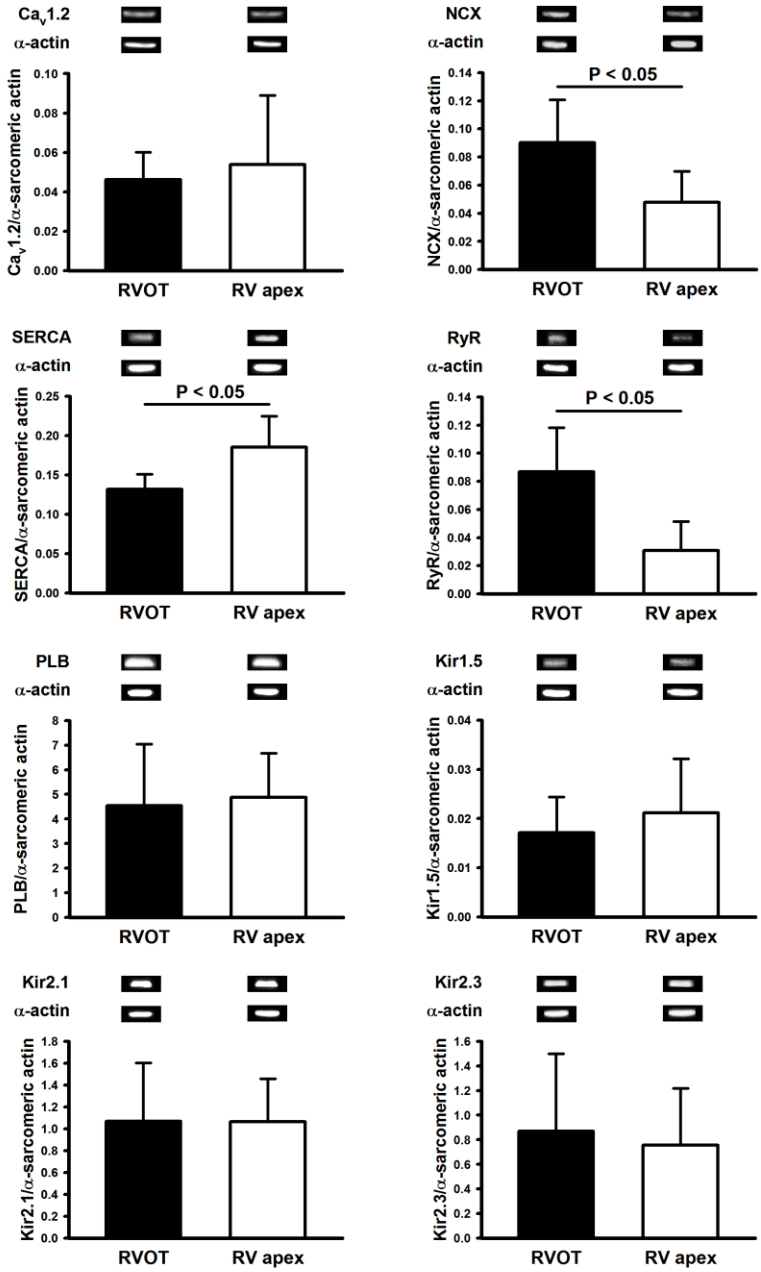
Cav1.2
α-actin
Cav1.2/α-sarcomeric actin
RVOT
RV apex
NCX
α-actin
NCX/α-sarcomeric actin
P < 0.05
RVOT
RV apex
SERCA
α-actin
SERCA/α-sarcomeric actin
P < 0.05
RVOT
RV apex
RyR
α-actin
RyR/α-sarcomeric actin
P < 0.05
RVOT
RV apex
PLB
α-actin
PLB/α-sarcomeric actin
RVOT
RV apex
Kir1.5
α-actin
Kir1.5/α-sarcomeric actin
RVOT
RV apex
Kir2.1
α-actin
Kir2.1/α-sarcomeric actin
RVOT
RV apex
Kir2.3
α-actin
Kir2.3/α-sarcomeric actin
RVOT
RV apex

科技部補助計畫衍生研發成果推廣資料表

日期:2014/10/26

科技部補助計畫	計畫名稱: 探討高體溫引發Brugada症候群的細胞及離子流機轉之研究
	計畫主持人: 蔡青峰
	計畫編號: 101-2314-B-040-017-MY2　　學門領域: 心胸內科

無研發成果推廣資料

101 年度專題研究計畫研究成果彙整表

計畫主持人：蔡青峰	計畫編號：101-2314-B-040-017-MY2
計畫名稱：探討高體溫引發 Brugada 症候群的細胞及離子流機轉之研究	

成果項目			量化			單位	備註（質化說明：如數個計畫共同成果、成果列為該期刊之封面故事...等）
			實際已達成數（被接受或已發表）	預期總達成數(含實際已達成數)	本計畫實際貢獻百分比		
國內	論文著作	期刊論文	0	0	100%	篇	
		研究報告/技術報告	0	0	100%		
		研討會論文	0	0	100%		
		專書	0	0	100%		
	專利	申請中件數	0	0	100%	件	
		已獲得件數	0	0	100%		
	技術移轉	件數	0	0	100%	件	
		權利金	0	0	100%	千元	
	參與計畫人力（本國籍）	碩士生	0	0	100%	人次	
		博士生	0	0	100%		
		博士後研究員	0	0	100%		
		專任助理	1	1	100%		
國外	論文著作	期刊論文	1	2	100%	篇	
		研究報告/技術報告	1	2	100%		
		研討會論文	0	0	100%		
		專書	0	0	100%	章/本	
	專利	申請中件數	0	0	100%	件	
		已獲得件數	0	0	100%		
	技術移轉	件數	0	0	100%	件	
		權利金	0	0	100%	千元	
	參與計畫人力（外國籍）	碩士生	0	0	100%	人次	
		博士生	0	0	100%		
		博士後研究員	0	0	100%		
		專任助理	0	0	100%		

其他成果 (無法以量化表達之成果如辦理學術活動、獲得獎項、重要國際合作、研究成果國際影響力及其他協助產業技術發展之具體效益事項等，請以文字敘述填列。)	無

	成果項目	量化	名稱或內容性質簡述
科教處計畫加填項目	測驗工具(含質性與量性)	0	
	課程/模組	0	
	電腦及網路系統或工具	0	
	教材	0	
	舉辦之活動/競賽	0	
	研討會/工作坊	0	
	電子報、網站	0	
	計畫成果推廣之參與（閱聽）人數	0	

科技部補助專題研究計畫成果報告自評表

請就研究內容與原計畫相符程度、達成預期目標情況、研究成果之學術或應用價值（簡要敘述成果所代表之意義、價值、影響或進一步發展之可能性）、是否適合在學術期刊發表或申請專利、主要發現或其他有關價值等，作一綜合評估。

1. 請就研究內容與原計畫相符程度、達成預期目標情況作一綜合評估

■達成目標

□未達成目標（請說明，以 100 字為限）

□實驗失敗

□因故實驗中斷

□其他原因

說明：

2. 研究成果在學術期刊發表或申請專利等情形：

論文：□已發表 □未發表之文稿 ■撰寫中 □無

專利：□已獲得 □申請中 ■無

技轉：□已技轉 □洽談中 ■無

其他：（以 100 字為限）

3. 請依學術成就、技術創新、社會影響等方面，評估研究成果之學術或應用價值（簡要敘述成果所代表之意義、價值、影響或進一步發展之可能性）（以 500 字為限）

本實驗希望藉著心電生理的基礎研究，探討在藉由模擬基因缺陷的 Brugada 動物模式中，研究溫度影響 Brugada 心電圖表現的細胞及離子流機轉及導致心室性心律不整的機轉，預估研究結果有助於了解 Brugada 症候群的致病機轉，以及高體溫(發燒)在心室性心律不整脈所扮演的角色及致病機轉，可以擴展對心律不整的細胞電氣生理學知識。且可有助於 Brugada 症候群的治療藥物或方法。同時可擴展對動作電位及鈣離子調控與電生理特性之關聯性心血管的細胞生理學的知識以及可以了解溫度及性別對於各種細胞離子流、鈣離子調控、電生理特性的影響。預計此研究成果未來可發表在國際知名 SCI 期刊論文。